Materials Science in Semiconductor Processing 166 (2023) 107733

Contents lists available at ScienceDirect

Materials Science in Semiconductor Processing

journal homepage: www.elsevier.com/locate/mssp

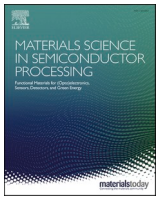

# Thickness dependence of dielectric properties of $TlGaS_2$ thin films

Z. Cicek [a], S. Yakut [b,**], D. Deger [b], D. Bozoglu [b], S. Mustafaeva [c], P. Ismailova [c], A.A. Hasanov [c], K. Ulutas [b,*]

[a] Physics Department, Institute of Graduate Studies in Sciences, Istanbul University, Istanbul, Turkey
[b] Physics Department, Faculty of Science, Istanbul University, Istanbul, Turkey
[c] Institute of Physics, National Academy of Sciences of Azerbaijan, Baku, Azerbaijan

ARTICLE INFO

*Keywords:*
$TlGaS_2$
Thin-film
Dielectric spectroscopy
Thickness dependence
AC conductivity

ABSTRACT

Bulk $TlGaS_2$ single crystals were produced by the Bridgman method. $TlGaS_2$ thin film samples were deposited from bulk crystals by the thermal evaporation technique under a high vacuum. $TlGaS_2$ thin films were deposited in the 100–750 nm thickness range. Dielectric spectroscopy measurements were operated in the frequency range of 1–$10^5$ Hz and temperature range of 273–373 K under the voltage of 1 V (rms). $TlGaS_2$ thin films have amorphous. Bulk $TlGaS_2$ has a crystalline structure based on X-Ray diffraction patterns. Three polarization mechanisms were detected from the analysis of Cole-Cole plots. At low frequencies, the effect of interfacial polarization was observed. Toward higher frequencies, two dipolar polarization mechanisms were detected. In comparison to the bulk $TlGaS_2$ single crystal, the dielectric constant of the thin films has 100–1000 times larger values at frequencies lower than 100 Hz. The thickness limit at which bulk physical properties started has been investigated. The transition thickness between bulk/thin film properties was detected at around 700 nm. The low dielectric constant and the good conductivity around $10^{-8}$ S/cm at$10^5$ Hz can give opportunities to use these thin films in technological applications.

## 1. Introduction

Semiconductor $TlGaS_2$ crystals have a layered structure and belong to the $TlGaX_2$ (X = S, Se, Te) $A^3B^1C_2^6$ type chemical compounds group [1–4]. In these layered crystals, while there are van der Waals bonds between the atoms that make up the layer, there are ionic and covalent bonds between the layers [5]. Semiconductor $TlGaX_2$ compounds have anisotropic and ferroelectric properties [6,7]. In recent years, the semiconductor $TlGaX_2$ triple compound has been an important subject of study in terms of meeting the need for optoelectronic applications due to its remarkable physical and chemical properties. The dielectric, electric, photoelectric, photovoltaic, and thermoluminescence properties of this compound were examined [2,4–8]. Mustafaeva studied the dielectric properties and ac conductivity of bulk $TlGaS_2$ single crystal prepared in the frequency ranges of $5.10^4$-$3.10^7$ Hz and 300 K temperature. It was found that the permittivity of the material was between 26 and 30. It was calculated The state's intensity, hopping distance, and time at the Fermi level in this study [9]. Kawabata et al. produced bulk $TlGaS_2$ compounds in different thicknesses, using the Bridgman method. They studied the dielectric properties and the transitions between the bands. Density function theory (DFT) for $TlGaS_2$ was obtained using an electronic band structure [10]. Asadov et al. have studied the dielectric properties of $TlGaS_2$ single crystal under electron irradiation [3]. Also, there are some studies on $TlGaS_2$ and compounds including $TlGaS_2$ [11–13]. In studies conducted on this subject, whole studies on the physical properties of $TlGaS_2$ are including the investigation in the bulk form [14–22]. In the literature, there is only one recent study on $TlGaS_2$ thin films. In the study, structural and optical properties of $TlGaS_2$ thin films in a thickness range of 100–200 nm were investigated [23].

In this study, $TlGaS_2$ thin films with different thicknesses between 100 and 750 nm were obtained using the thermal evaporation method. The capacity and loss values of these samples were determined by using dielectric spectroscopy in the frequency range of 1Hz–20 MHz at a temperature interval of 273–373 K. It was observed that there is a lack of information on the dielectric properties of $TlGaS_2$ thin films in literature. For this reason, it is aimed to contribute to the literature by studying the dielectric properties of $TlGaS_2$ thin films depending on frequency, temperature, and thickness. Dielectric properties and electrical

* Corresponding author.
** Corresponding author.
*E-mail addresses:* yakuts@istanbul.edu.tr (S. Yakut), hku@istanbul.edu.tr (K. Ulutas).

https://doi.org/10.1016/j.mssp.2023.107733
Received 12 June 2022; Received in revised form 13 June 2023; Accepted 8 July 2023

characteristics of some ternary compounds having a similar composition to $TlGaS_2$ were studied. In these studies, the structure and dielectric behavior of $TlSbS_2$ bulk and thin films [24], dielectric properties and AC conductivity of $TlSbTe_2$ thin films [25], and electrical switching in $TlSbSe_2$ compounds [26] were investigated. The results belonging to $TlGaS_2$ thin film samples will be evaluated contrary to studies performed on bulk materials in literature. The thickness at which thin-film characteristics differ from bulk characteristics will be examined. In this way, the use of thin films of $TlGaS_2$ is possible as an alternative in nano or micro-sized applications of $TlGaS_2$ bulk materials. The investigation of the dielectric properties of $TlGaS_2$ thin films will be a complete study of the literature in which the structural and optical properties of TlGaS2 thin films were evaluated. Thus, an electrical evaluation on $TlGaS_2$ thin films will be done. The interpretation of thickness-dependent dielectric properties of $TlGaS_2$ thin films will give information about the application of these materials in various areas in daily life electronics, microengineering, thermo-electric industry, electronic applications and optical limiting applications.

## 2. Experimental

### 2.1. Production of thin-film samples

Bulk $TlGaS_2$ samples were prepared using the Bridgman technique which is described in the literature [13,27,28]. $TlGaS_2$ single crystal bulk samples were produced using appropriate elemental mixtures. These mixtures were melted at 1000 ± 5 K for 5–7 h in silica tubes which were sealed off under a vacuum of $7{,}5 \times 10^{-6}$ Torr. $TlGaS_2$ single crystal bulk samples were homogenized by vacuum annealing at 750 K for 120 h. The annealed samples were furnace-cooled to room temperature. The chemicals [Thalium (Tl), Galium (Ga), Sulphur (S)] used in the bulk production process have a purity of 99,99% [3]. As mentioned in the introduction part, the article is aimed to compare the dielectric properties of thin film $TlGaS_2$ and bulk single-crystal $TlGaS_2$ samples. Because of this purpose, the bulk $TlGaS_2$ samples produced by some authors of this article for a previous study were used to produce thin film $TlGaS_2$ samples [3,9,28].

The picture of $TlGaS_2$ single crystal samples is seen in Scheme 1. The flowchart and the information including the procedures of the Bridgman Stockbarger technique are presented in previous literature [3,9,28] (see Scheme 2).

Thin-film samples were deposited in three steps in the shape of parallel plated capacitor form using suitable masks to investigate the dielectric properties. Whole thin film deposition processes were operated by thermal evaporation under $10^{-5}$ Torr pressure. Microscope slides were as substrates. The microscope slides (25.4 mm–76.2 mm) were cleaned using pure water (resistivity of 15 MΩ cm), acetone (Merck), and ethanol (Merck), respectively, with the help of an ultrasonic cleaner. As the first step of deposition, Aluminum (Al) was evaporated as the lower electrode. Then, $TlGaS_2$ thin films were coated on the Al lower electrode. The deposition of $TlGaS_2$ thin films was operated by wearing a charcoal mask to be protected from the poisonous effects of thallium (Tl). $TlGaS_2$ thin films having thicknesses of

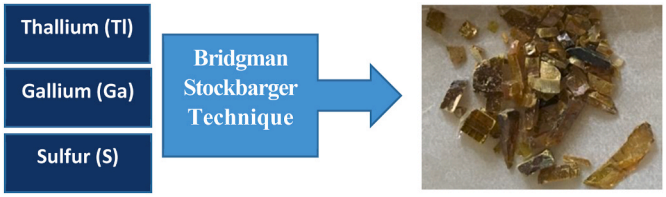


**Scheme 1.** Production of $TlGaS_2$ single crystal samples.

### 2.2. Thermal evaporation technique

100, 250, 500, and 750 nm were produced. As the last step of sample production, the upper electrodes were deposited under the same conditions similar to the lower electrodes. The thicknesses of the Al electrodes were defined as 300 nm. The thicknesses of both electrodes and $TlGaS_2$ thin films were determined by the geometrical method. So, the $Al/TlGaS_2/Al$ samples were prepared in capacitive form. The surface area of capacitor samples was measured by a micrometer. The surface area of the thin film samples was measured by a traveling microscope and was determined as 16 $mm^2$.

### 2.3. X-ray diffraction (XRD) analysis

The morphology of the $TlGaS_2$ samples was defined by XRD analysis by Rigaku D/Max-2200/PC having Cu-Kα (λ = 1.54 Å) radiation source. The analysis is progressed based on 2θ angles between 0 and 90° at room temperature. The XRD analysis was operated on $TlGaS_2$ crystal and all thin film samples.

### 2.4. Attenuated total reflection fourier transformed infrared spectroscopy (ATR FT-IR) analysis

ATR FT-IR analysis was operated as an attenuated reflection technique over 400-4000 $cm^{-1}$ on $TlGaS_2$ crystal and all $TlGaS_2$ thin film samples by FT/IR-4700typeA device due to ATR-PRO-ONE accessory at room temperature. Measurement results present information about the structural differences, coming from the deposition conditions, between bulk and thin film samples.

### 2.5. Dielectric spectroscopy measurements

The samples have a parallel plate capacitor form of $Al/TlGaS_2/Al$. Thin-film form samples were placed on a dielectric spectroscopy device (Alpha-A High-Resolution Dielectric, Conductivity, and Impedance Analyzer). The frequency range was determined as $10–10^6$ rad/s (≈$1–10^5$ Hz) and the temperature range was selected as 273–373 K. Frequency, temperature and thickness-dependent capacity, and loss values of the $TlGaS_2$ films were measured.

## 3. Results and discussion

### 3.1. Structural characterization of $TlGaS_2$ crystal and $TlGaS_2$thin films

#### 3.1.1. XRD analysis

XRD patterns for bulk $TlGaS_2$ and $TlGaS_2$ films are shown in Fig. 1. It is detected that the $TlGaS_2$ crystal represents characteristic peaks belonging to $TlGaS_2$ [23,28,29]. Whole thin film samples have amorphous while the bulk sample has a crystalline structure. The results of representative thin film samples with thicknesses of 250 nm and 750 nm are given in Fig. 1. The crystal structure changes to amorphous by thermal evaporation as observed in studies operated on some binary and ternary compounds [23–25,30,31]. For most samples, it is a fact that thin-film deposition causes the splitting of solid crystal structure into vapor molecules before depositing on the substrate. Then, vapor molecules of the sample are deposited on the substrate in a custom way. Thus, a continuous crystalline structure except in some regions can not be obtained during deposition. This non-crystalline structure can be called amorphous [23,32–35].

#### 3.1.2. ATR FT-IR analysis

ATR FT-IR analysis of $TlGaS_2$ crystal corresponds to the spectrum obtained for $TlGaS_2$ in literature [36,37]. It can be observed that the characteristic transmission bands become undetectable for thin film samples as shown in Fig. 2. Also, new bands appear in spectra. The crystal structure changes to amorphous. These results coincide with XRD

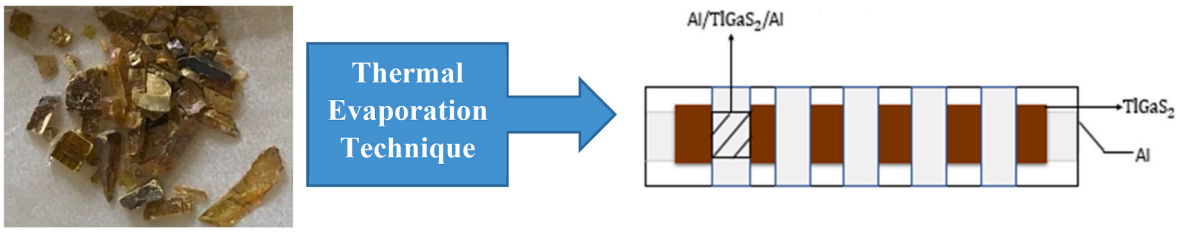


**Scheme 2.** The production of $TlGaS_2$ thin films from bulk $TlGaS_2$ samples by thermal evaporation.

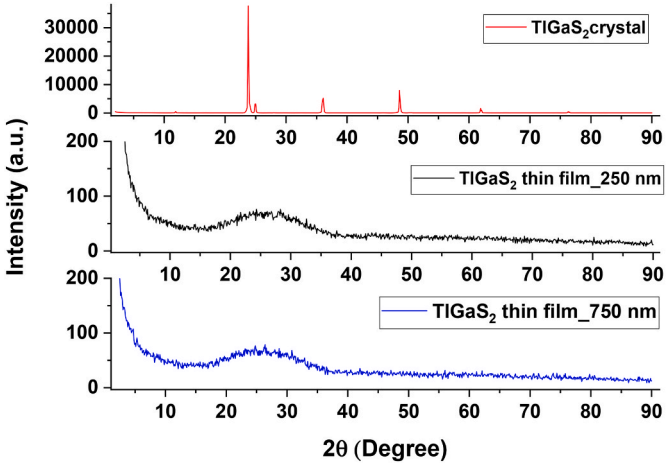


**Fig. 1.** XRD pattern for $TlGaS_2$ crystal (The granule of the sample before deposition), $TlGaS_2$ thin films with thicknesses of 250 and 750 nm.

results. On the vertical axis, the change from crystalline to amorphous phase causes an increase in the transmission of incoming light. The transmission increases with increasing film thickness. The increasing effect of thickness can be interpreted by The presence of closer packing in structure with increasing density. The increasing effective density may trigger the orientation and the ordering of crystallite regions increases [38,39].

### 3.1.3. *Dielectric analysis*

*3.1.3.1. Frequency and temperature dependence of dielectric constant.* The dielectric constant values of $TlGaS_2$ thin films were calculated from measured capacitance with a parallel plate of the sample capacitor by using equation (1):

$$\kappa' = \frac{Cd}{\varepsilon_0 A} \tag{1}$$

where κ' is the dielectric constant, d film thickness, C is the capacitance of the capacitor, A is the surface area of the electrode, and $\varepsilon_0$ permittivity of free space [40]. In Fig. 3, it is shown that the dielectric constant values are frequency and temperature-dependent for all $TlGaS_2$ thin films. It is seen that the dielectric constant decreases with increasing frequency and exhibits an increase in temperature. Polarization mechanisms in the structure were detected by the fitting results of the Cole-Cole equation which is described below,

$$\frac{\kappa^*(\omega) - \kappa_\infty}{\Delta\kappa} = \frac{1}{1 + (i\omega\tau_{CC})^\beta} \tag{2}$$

where, κ* is the complex dielectric function, $\kappa_\infty$ is the dielectric constant at infinitely high frequencies, Δκ is the dielectric strength which is the difference between the static dielectric constant and the dielectric constant at infinitely high frequencies. ω is the angular frequency, $\tau_{CC}$ is relaxation time and β is the coefficient of broadening of polarization inside the frequency range [29,41]. Two polarization mechanisms were determined in the investigated frequency and temperature interval. It is detected that these mechanisms are temperature-dependent and shift toward higher frequencies with increasing temperature. One of these polarization mechanisms is more pronounced at high temperatures and inside angular frequency regions of 1–$10^3$ rad/s (represented by blue fit lines). The other one is observed clearly at low temperatures and inside the angular frequency region of 1000–$10^6$ rad/s (represented by red fit lines). The polarization mechanism observed at low frequencies and high temperatures has a relaxation time between $10^{-2}$ and $10^{-1}$ s, while the mechanism observed at relatively higher frequencies and lower temperatures has a relaxation time between $10^{-4}$ and $10^{-2}$ s. The remarkable difference between relaxation times may indicate the difference between the nature of these two mechanisms. As known from the literature, from low frequencies to high frequencies electrical polarization mechanisms appear as steps starting from space-charge (interfacial) polarization. Following space-charge polarization, dipolar polarization, ionic polarization, and electronic polarization, respectively [42–44]. The mechanism observed at angular frequencies between 1 and $10^3$ rad/s (≈1 and 100 Hz) can be attributed to interfacial or electrode polarization [36–38,45–48]. The other mechanism which is detected in the frequency range of 1000–$10^6$ (≈100–$10^5$ Hz) can be attributed to dipolar polarization [37,47,49]. It was reported that there is not any remarkable relaxation in the frequency range for a single crystal [9], while there are two relaxation mechanisms detected from dielectric constant plots for $TlGaS_2$ thin film samples. This difference is sourced from the change of crystal structure by thin film deposition. In thin film samples, two relaxation mechanisms. One be attributed to space-charge polarization at low frequencies which is sourced from partly free charge carriers produced by thin film deposition. The other mechanism is called dipolar polarization of covalent bonding in structure [44,49,50]. This evaluation supports the interpretation written from XRD results.

The dielectric constant has values around 9 and 11 for thin-film samples with thicknesses of 100 nm and 500 nm at room temperature, respectively. However, the dielectric constant is between 25 and 30 at room temperature and 10 kHz for $TlGaS_2$ single crystal in literature [1]. The difference between dielectric constant values for thin-film $TlGaS_2$ and $TlGaS_2$ single-crystal samples can be related to the nature of thin-film deposition as interpreted in structural analysis. At the time of deposition, the placing of vapor may succeed to construct the solid crystal structure in some regions on the substrate, but from a general view, it is possible to obtain an amorphous or a polycrystalline structure [51–53]. Thus, the crystal structure changes, and new bonds and some excess, partially free charge carriers may occur in the structure. This new structure can include different polarization mechanisms by comparing the single-crystal structure. Amorphous thin film products which are deposited from binary and ternary compounds may have higher dielectric constants than bulk binary and ternary compounds [44,54]. Partially free charge carrier occurs because the deposition process may be subjected to space-charge polarization which is dominant frequencies lower than 100 Hz. In our article, it is observed that there is a frequency and temperature-dependent behavior of dielectric constant as shown in Fig. 3. When the frequency and temperature-dependent

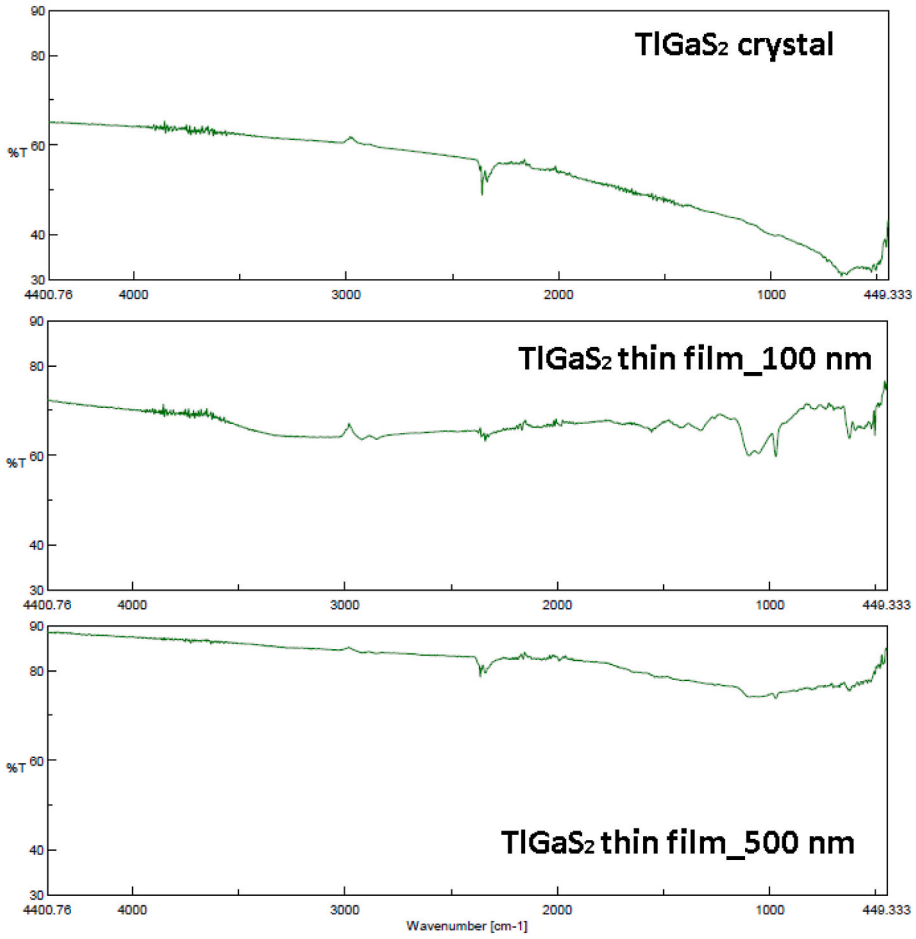


**Fig. 2.** ATR FT-IR spectra for $TlGaS_2$ crystal, $TlGaS_2$ thin films with thicknesses of 100 nm and 500 nm.

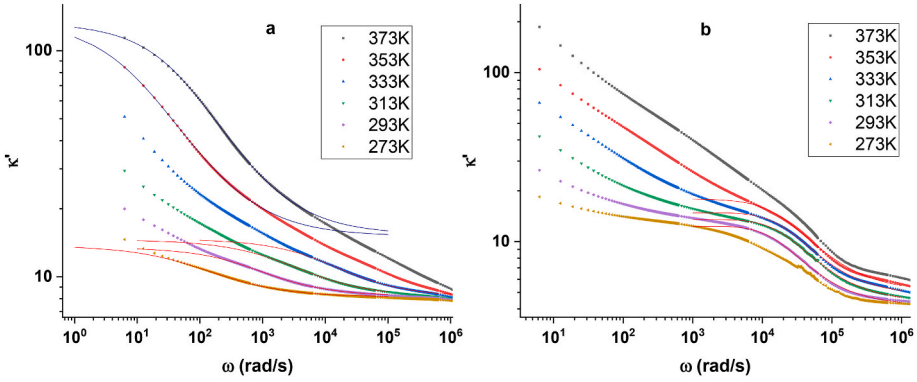


**Fig. 3.** Frequency and temperature dependence of dielectric constant (κ') for samples with thicknesses of a) 100 nm, b) 500 nm as representative samples.

dielectric constant of bulk $TlGaS_2$ is considered [9], the dielectric constant has values between 25 and 30 at frequencies lower than $10^4$ Hz. In response to this, the dielectric constant values obtained in our study have values between 100 and 1000 depending on the thickness as shown in Fig. 3. As a consequence of this observation, the remarkable increase of the dielectric constant of thin film samples at low frequencies may give ideas to use this thin film material in applications except the areas at which the bulk form is used.

*3.1.3.2. Thickness dependence of dielectric constant of $TlGaS_2$ thin films.* The variation of the dielectric constant depending on the film thickness is given in Fig. 4. It is shown that the dielectric constant increases exponentially between 5 and 10 with increasing thickness at 1 kHz at room temperature. However, when a certain thickness value is reached, it is seen that the dielectric constant becomes thickness independent at 1 kHz between 600 and 800 nm. Similar behavior depending on thickness is observed for all frequencies. The exponential fit equation calculates the thickness-independent dielectric constant around 11 at a thickness of 1 μm. The amount of void density that decreases with the increase of thickness will be too small to affect the polarization in the structure after a certain thickness and over this thickness the sample is called bulk [25]. The reason for the dielectric constant with increasing thickness is based on the decrease in free volume [25,51]. As mentioned in Fig. 2, the transmission increases with increasing thickness, and the reason for this

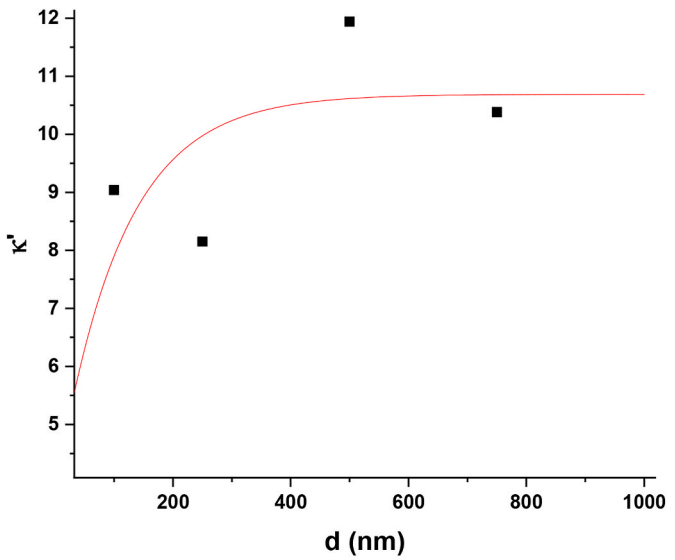


**Fig. 4.** Thickness dependence of dielectric constant at 293 K and 1 kHz.

increase is related to the ordering of crystallite regions. Crystallite regions can be assumed as regions occupied by a high number of charge carriers instead of voids. Thus, the density of voids decreases with increasing thickness. A high number of charge carriers represent a higher dielectric constant as observed in Fig. 4. It can be said that the thickness-dependent dielectric constant behavior supports the result obtained in the ATR FT-IR spectrum depending on the thickness of $TlGaS_2$ thin films.

*3.1.3.3. Frequency and temperature dependence of dielectric dissipation (tanδ) of $TlGaS_2$ thin films.* Three polarization regions can be seen in Fig. 5. These three mechanisms can be classified as region1 for the mechanism observed at frequencies lower than 100 Hz and fitted by blue lines; region2 for the mechanism observed at higher frequencies than 100 Hz and fitted by black lines; region3 for the mechanism observed at low temperatures, frequencies higher than the frequencies, which the region2 is detected, and fitted by red lines. While the region1 can be related to interfacial polarization or electrode polarization, the other two mechanisms observed at the relatively higher frequency side at high temperatures (represented by black fit lines) and the high-frequency side at low temperatures (represented by red fit lines) can be related to dipolar polarization of parts of the lattice with different size [41,55,56]. The relaxation time obtained from Cole-Cole fits applied to tanδ plots for all mechanisms can be classified as a relaxation time for region1 is detected between $10^{-2}$ and $10^{-1}$ s; for region2 it is between $10^{-2}$ and $10^{-1}$ s at lower temperatures than of region1, that is at same temperatures it can be said that relaxation time may be lower than of region1; for region3 the relaxation time is around $10^{-4}$ s. These results can be evaluated that region2 and region3 have similar natures and probably these mechanisms are dipolar polarization mechanisms. The difference may be the size of the polarized charge carriers.

*3.1.3.4. Frequency and temperature dependence of AC conductivity ($\sigma_{AC}$).* AC conductivity ($\sigma_{AC}$) with the equation as:

$$\sigma'(\sigma_{AC}) + i\sigma'' = \omega\varepsilon_0\kappa'' + i\omega\varepsilon_0\kappa' \quad (3)$$

where σ' is the real part of conductivity and called AC conductivity ($\sigma_{AC}$), σ'' is the imaginary part of total conductivity [57]. $\sigma_{AC}$ in equation (4):

$$\sigma_{AC} = \sigma_0 + A\,\omega^s \quad (4)$$

where $\sigma_0$ is frequency-independent conduction. It is observed on the low-frequency side. A is a coefficient and s is a coefficient that relies on the type of conduction mechanism [25,42,52,58–61]. σ'' can be used if there is an unknown polarization mechanism at frequencies lower than 100 Hz [57,62]. In this region, there may be trouble distinguishing interfacial polarization from electrode polarization [29,54]. In Fig. 6, the frequency and temperature dependence of AC conductivity for all samples can be seen. It is shown that there are three polarization or conduction mechanisms in the investigated frequency and temperature interval. The mechanism observed at frequencies lower than $10^3$ rad/s ($\approx 10^2$ Hz) can be attributed to interfacial polarization or electrode polarization. This mechanism is represented by blue fit lines. To distinguish the nature of the region1, the frequency dependence of σ'' can be used at room temperature.

The presence of electrode polarization can be detected by analyzing the temperature dependence of σ'' at room temperature. If there is an influence of electrode polarization at low frequencies, there should be a relaxation behavior as a hill or as a shoulder at frequencies lower than 1000 rad/s or 100 Hz [57]. Fig. 7 shows that there is not any sign of the presence of electrode polarization. Thus, it can be evaluated that at frequencies lower than 100 Hz interfacial polarization dominates total polarization.

In Fig. 8 s values for region2 and region3 can be shown. The temperature dependence of s can give information about the type of conduction. The black data points represent the region2 and except the plot c (temperature-dependent s values for the sample with a thickness of 500 nm) s values are lower than 1 and around 0,8 and 0,6 (for the sample with a thickness of 750 nm) s values are temperature independent. This behavior supports the quantum mechanical tunneling (QMT) conduction mechanism [53,63]. For plot c (plot of the sample with a thickness of 500 nm) s values are larger by a bit of 1, than with increasing temperature s values decrease. This behavior corresponds to the classical

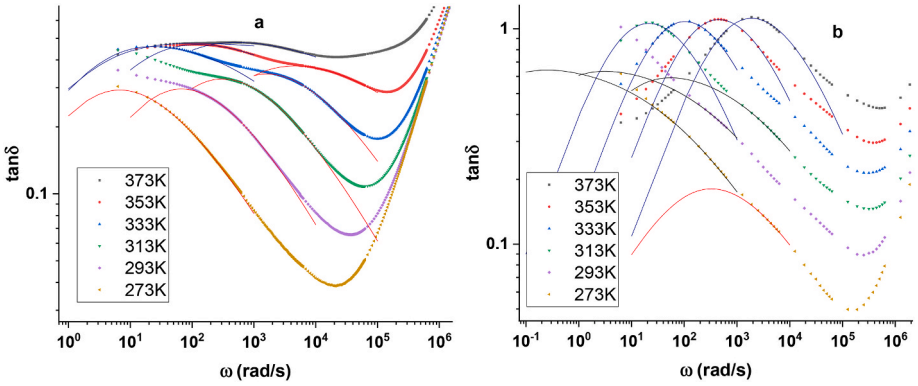


**Fig. 5.** Frequency and temperature dependence of dielectric dissipation (tanδ) for the samples with thicknesses of a) 250 nm and b) 750 nm as representative samples.

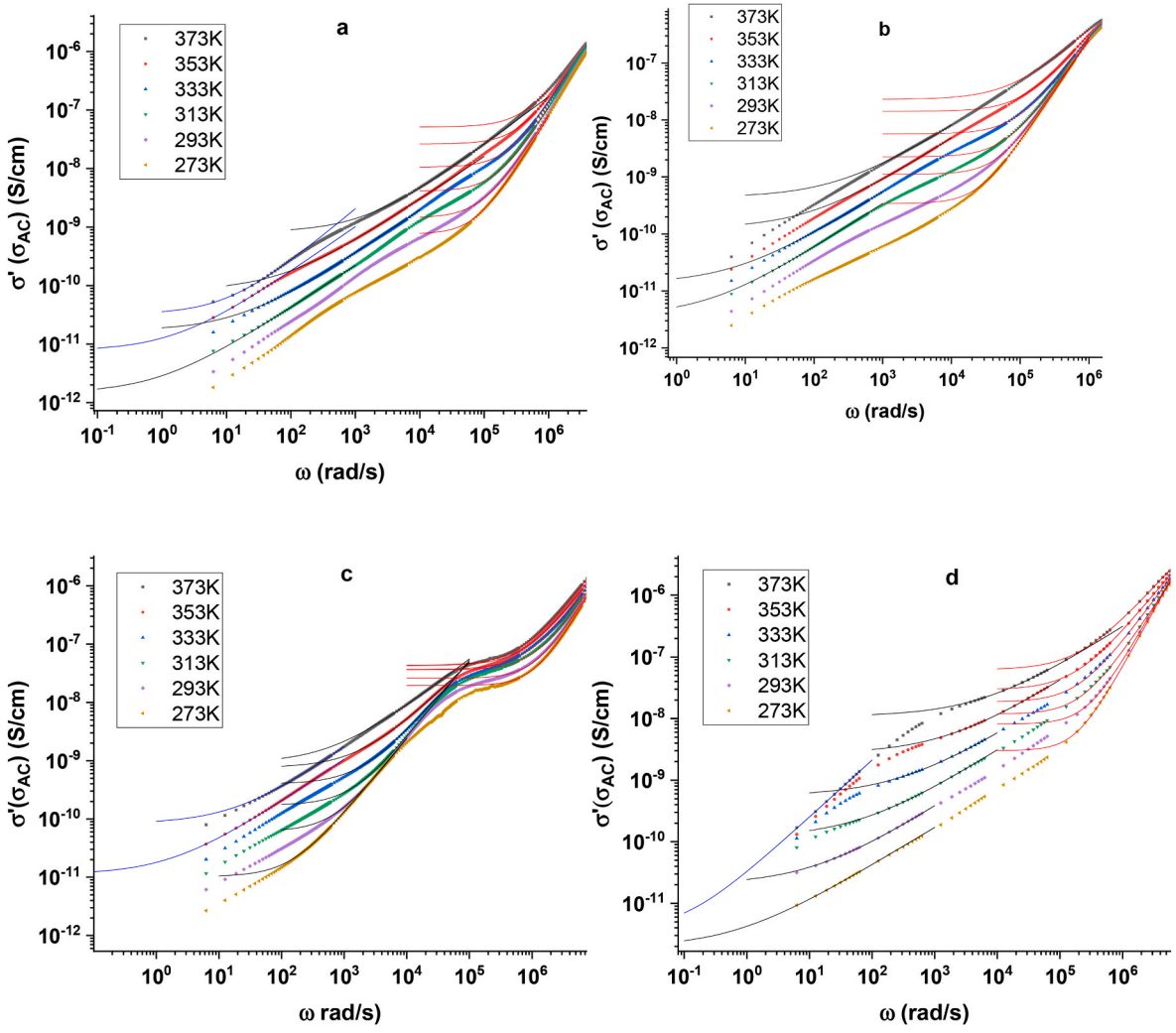


**Fig. 6.** Frequency and temperature dependence of AC cınductivity ($\sigma_{AC}$) for samples with thicknesses of a) 100 nm, b) 250 nm, c) 500 nm, d) 750 nm.

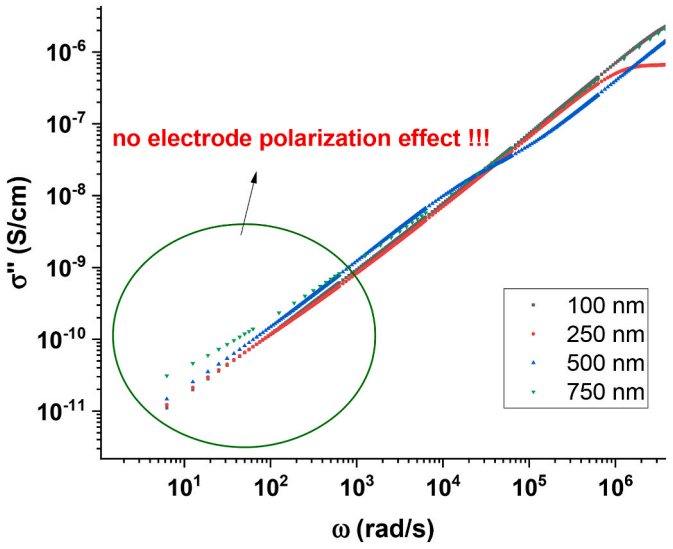


**Fig. 7.** Frequency dependence of imaginary part of conductivity (σ") at room temperature.

hopping of charge carriers. When s values for region 3 are investigated, it is observed that there is a decrease starting from 1,8 toward 1 with increasing temperature. This behavior can be attributed to the classical hopping mechanism [25,42,57,64]. However, it can be said that in Region 3 the charge carriers may be smaller in comparison to the size of charge carriers or polarized in Region 2 [57]. Although the dielectric constant of thin-film samples is lower than that of bulk $TlGaS_2$, $\sigma_{DC}$ or DC-like conductivity values at $10^5$ Hz frequency for region 3 are almost the same for thin film samples in comparison to that of bulk samples in literature [9]. Especially, for the 500 nm thin film sample the conductivity is larger a bit (larger than $10^{-8}$ S/cm) at $10^5$ Hz at room temperature. A lower dielectric constant and better or equal conductivity at high frequencies can make a better choice to use $TlGaS_2$ thin films in switching applications [17]. Also, equal conductivity can make $TlGaS_2$ thin films a better option in thermoelectric applications as nano-sized thermoelectric materials [65].

*3.1.3.5. Activation energies calculated for polarization regions.* To decide the type of polarization mechanisms, the activation energies are calculated from Equation (5):

$$\sigma_{AC} = \sigma_0 \, e^{-\frac{\Delta E}{k_B T}} \tag{5}$$

where $\sigma_0$ is the frequency-independent part of conductivity. It can be called DC-like conductivity. ΔE is activation energy which is the minimum thermal energy required to support the contribution of a charge

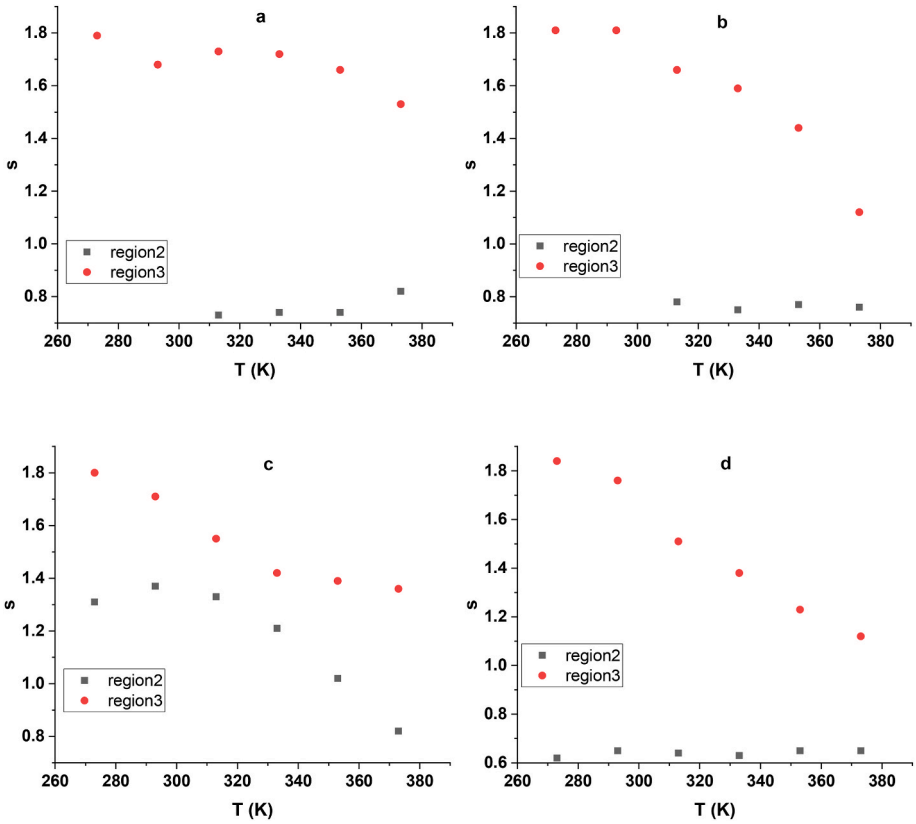


**Fig. 8.** Temperature dependence of s values for region2 and region3 for samples with thicknesses of a) 100 nm, b) 250 nm, c) 500 nm, d) 750 nm.

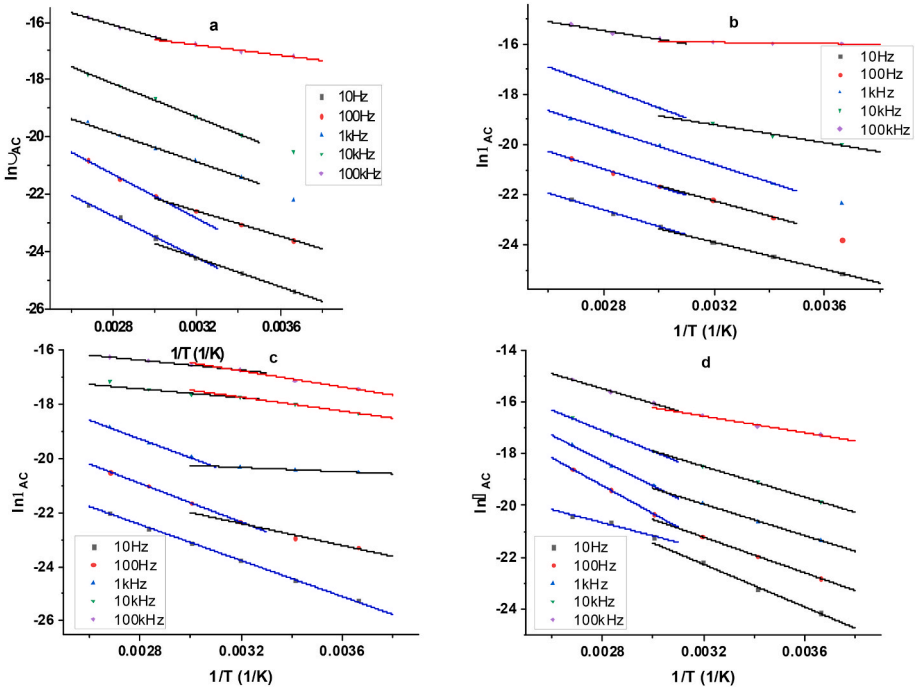


**Fig. 9.** Inverse temperature dependence of natural logarithm of AC conductivity for samples with thicknesses of a) 100 nm, b) 250 nm, c) 500 nm, d) 750 nm.

carrier to the conduction [52,57,59–61,66,67].

In Fig. 9 the application of this equation to temperature-dependent conductivity is shown. In constant frequency graphs of dielectric spectroscopy results usually, 1 kHz constant frequency is used to eliminate the possible effects of electrode polarization which is observed at frequencies around 100 Hz. In addition to the frequency, we used some other frequencies between 1-$10^5$ Hz. Similar to previous figures, blue fit lines are represented the polarization mechanism observed at high temperatures and low frequencies; black fit lines are attributed to the polarization mechanism observed at higher frequencies in the former

mechanism. Red fit lines represent the mechanism observed at high frequencies and low temperatures. When the calculated activation energies are compared for three polarization mechanisms, it is detected that the activation energy of the mechanism with blue fit lines is around 0,35 eV and changes depending on thickness. The activation energy of the mechanism with the black fit line is around 0,25 eV with changing thickness. This activation energy interval is the interval that orientational polarization that has been observed as mentioned in the literature [67–70]. The last mechanism represented with red fit lines has activation energy around 0,10 eV based on thickness change. This activation energy is close to the activation energy obtained for water-containing materials impedance analysis results [68,71]. These activation energies indicate the presence of dipolar polarization [39,55,60,72,73]. When Table 1 is detected, it can be seen that the activation energies increase with increasing thickness in general. The varying activation energies in the level of dipolar polarization may indicate the presence of varying sizes of charge groups appearing as a result of the thin film deposition process. There may be charge groups with different sizes as a result of the splitting of the $TlGaS_2$ lattice. Also, void density which depends on thickness can affect the polarizability of charge groups [74].

## 4. Conclusion

$TlGaS_2$ thin film samples with thicknesses of 100 nm, 250 nm, 500 nm, and 750 nm were deposited from bulk $TlGaS_2$ single crystals by thermal evaporation, under a high vacuum level. The morphological analysis based on XRD results shows that the $TlGaS_2$ crystal is crystalline as expected while the structure of thin-film samples is amorphous. ATR FT-IR results exhibit an increase in the order crystallite structure with increasing film thickness based on the increase in transmission. Dielectric measurements were operated by an impedance analyzer in the frequency range 1–$10^5$ Hz and temperature range 273–373 K. Analyze results showed that the dielectric constant of thin-film samples had values, as an average of 11, about half of the dielectric constant of bulk single crystal $TlGaS_2$. The value 11 reached around the thicknesses between 600 and 800 nm. Following this range, the dielectric constant becomes thickness independently. The range 600–800 nm is called the bulk behavior border for the dielectric properties of $TlGaS_2$ thin films. The thickness dependence of the dielectric constant supports the behavior observed in ATR FT-IR spectra. Starting from dielectric constant behavior to AC conduction behavior some analyzing plots were used and it was realized that there were three polarization mechanisms in the investigated frequency and temperature range for $TlGaS_2$ thin films. The mechanism observed at high temperatures and frequencies lower than 100 Hz was detected as interfacial polarization. The other two mechanisms observed at lower temperatures and higher frequencies were attributed to dipolar polarization. It is known that for single crystal $TlGaS_2$, it is possible one relaxation $^{behavior}$. However, for the thin-film form of $TlGaS_2$, it is possible to have three different polarization mechanisms. The reason may be the nature of the deposition process. Thermal evaporation causes the splitting of a solid into a vapor. Then, the vapor solidifies at the time of deposition on the substrate. The placement rate of atoms and molecules on the substrate restricts the occurrence of crystallization. Thus, a polycrystalline or amorphous structure is constructed. As a result, the structure may have additional partially free charge carriers and dipolar groups of different sizes. The presence of interfacial polarization indicates the effect of partially free charge carriers at frequencies below 100 Hz. This can increase the conduction of thin-film samples at which in application areas requiring better electrical conduction. Also on the low-frequency side, the dielectric constant has values between 100 and 1000 which is larger than the dielectric constant of bulk samples at similar frequencies. $TlGaS_2$ thin films can be applied in areas such as optoelectronics, photovoltaic, and thermoelectric. The lower dielectric constant and the relatively good conductivity of $10^{-8}$ S/cm at $10^5$ Hz compared to the dielectric constant and the conductivity of $TlGaS_2$ bulk single crystal form may give advantages to $TlGaS_2$ thin films in thermoelectric and switching applications. The investigation of thickness-dependent characteristics of $TlGaS_2$ thin film can give options to evaluate possible alternative applications in nano or micro-sized applications of $TlGaS_2$ bulk materials such as electronics, microengineering, thermo-electric industry, electronic applications, and optical limiting applications. Also, the investigation of the dielectric properties of $TlGaS_2$ thin films will be a complete study of the literature in which the structural and optical properties of TlGaS2 thin films were evaluated.

**Table 1**
The activation energies calculated from fit lines with colors of black, blue, and red depending on $TlGaS_2$ film thicknesses.

| $TlGaS_2$ thin film thickness (nm) | Activation energy fitted by (eV) | | |
|---|---|---|---|
| | Black fit lines | Blue fit lines | Red fit lines |
| **100** | 0,22 | 0,32 | 0,070 |
| **250** | 0,24 | 0,30 | 0,070 |
| **500** | 0,17 | 0,30 | 0,075 |
| **750** | 0,26 | 0,40 | 0,13 |

## CRediT authorship contribution statement

**Z. Cicek:** Writing – original draft, Resources, Data curation. **S. Yakut:** Writing – review & editing, Resources, Data curation. **D. Deger:** Writing – review & editing, Visualization, Supervision. **D. Bozoglu:** Resources, Data curation. **S. Mustafaeva:** Resources. **P. Ismailova:** Resources. **A.A. Hasanov:** Resources. **K. Ulutas:** Writing – review & editing, Visualization, Supervision.

## Declaration of competing interest

The authors declare that they have no known competing financial interests or personal relationships that could have appeared to influence the work reported in this paper.

## Data availability

Data will be made available on request.

## Acknowledgments

Thanks to Professor Elmira Kerimova (R.I.P.) for her contribution to this study. This study was supported by the Scientific Research Projects Coordination Unit of Istanbul University under project numbers 26491, 26463, 3569, 30048, 38322, and 37896.

## References

[1] S.N. Mustafaeva, Frequency effect on the electrical and dielectric properties of (TlGaS 2) 1 - X (TlInSe 2) x (x = 0.005, 0.02) single crystals, Inorg. Mater. 46 (2010) 108–111, https://doi.org/10.1134/S0020168510020032.
[2] S. Asadov, S.M.-P. of the S. State, U, Dielectric losses and charge transfer in antimony-doped TlGaS2 single crystal, Semiconductors 60 (2018) (2018) 495–498, https://doi.org/10.1134/S1063783418030034.
[3] S.M. Asadov, S.N. Mustafaeva, V.F. Lukichev, Modifying the dielectric properties of the TlGaS2 single crystal by electron irradiation, Russ. Microelectron. 49 (2020) 281–286, https://doi.org/10.1134/S1063739720040022.
[4] S. Delice, M. Isik, N.M. Gasanly, Thermoluminescence properties and trapping parameters of TlGaS 2 single crystals, J. Lumin. 244 (2022), 118714, https://doi.org/10.1016/j.jlumin.2021.118714.
[5] B. Gürbulak, S. Duman, A. Ateş, The Urbach tails and optical absorption in layered semiconductor TlGaSe2 and TlGaS2 single crystals, Czech. J. Phys. 55 (2005) 93–103, https://doi.org/10.1007/S10582-005-0011-4.
[6] A.U. Sheleg, V.G. Gurtovoi, V.V. Shevtsova, S.N. Mustafaeva, E.M. Kerimova, Effect of ionizing radiation on the dielectric characteristics of TlInS 2 and TlGaS 2 single crystals, Phys. Solid State 54 (2012) 1870–1874, https://doi.org/10.1134/S1063783412090284.
[7] V. Hurtavy, A. Sheleg, S.M.-P. of the S., U, The electric conductivity and dielectric properties of Tl (GaS 2) 1–x (InSe 2) x solid solutions, Semiconductors 59 (2017) (2017) 1479–1483, https://doi.org/10.1134/S106378341708011X.

[8] M. Açikgöz, P. Gnutek, C. Rudowicz, Modeling local distortions around Fe3+ ions doped into TlGaS2 crystal using superposition model analysis of the zero-field splitting parameters, Solid State Commun. 150 (2010) 1077–1081, https://doi.org/10.1016/J.SSC.2010.03.008.

[9] S.N. Mustafaeva, Frequency dispersion of dielectric coefficients of layered TlGaS 2 single crystals, Phys. Solid State 46 (2004) 1008–1010, https://doi.org/10.1134/1.1767234.

[10] T. Kawabata, Y. Shim, K. Wakita, N. Mamedov, Dielectric function spectra and inter-band optical transitions in TlGaS2, Thin Solid Films 571 (2014) 589–592, https://doi.org/10.1016/J.TSF.2014.02.100.

[11] B.A. Ünlü, A. Karatay, E. Akhuseyin Yildiz, T. Dinçbay, H. Ünver, N. Gasanly, A. Elmali, Defect assisted nonlinear absorption and optical limiting in amorphous TlGaS 2(1-x) Se 2(x) ($0 \leqslant x \leqslant 1$) thin films, J. Lumin. (2021), https://doi.org/10.1016/j.jlumin.2021.118540.

[12] Z. Sahan, Ö. Akkuş, S. Berber, Spin polarized edge states in TlGaS2 nanoribbons, Phys. B Phys. OfCondensed Matter. 639 (2022), https://doi.org/10.1016/j.physb.2022.413979.

[13] M. Isik, · M. Terlemezoglu, · N.M. Gasanly, · R.F. Babayeva, Vibrational modes in (TlGaS 2) x-(TlGaSe 2) 1−x mixed crystals by Raman measurements: compositional dependence of the mode frequencies and line-shapes, J. Mater. Sci. Mater. Electron. 31 (1234) (2020) 14330–14335, https://doi.org/10.1007/s10854-020-03990-8.

[14] M. Isik, E. Bulur, N.M. Gasanly, Low-temperature thermoluminescence in TlGaS2 layered single crystals, J. Lumin. 135 (2013) 60–65, https://doi.org/10.1016/j.jlumin.2012.10.025.

[15] O. Karabulut, K. Yilmaz, B. Boz, Electrical and optical properties of Co doped TlGaS2 crystals, Cryst. Res. Technol. 46 (2011) 79–84, https://doi.org/10.1002/crat.201000486.

[16] F.V. Pérez, R. Cadenas, C. Power, J. González, C.J. Chervin, Raman scattering and phase transition in TlGaS2 under pressure, J. Appl. Phys. 101 (2007), https://doi.org/10.1063/1.2472649.

[17] A.A. Al Ghamdi, A.T. Nagat, F.S. Bahabri, R.H. Al Orainy, S.E. Al Garni, Study of the switching phenomena of TlGaS 2 single crystals, Appl. Surf. Sci. 257 (2011) 3205–3210, https://doi.org/10.1016/j.apsusc.2010.10.140.

[18] L. Nemerenco, N.N. Syrbu, V. Dorogan, N.P. Bejan, V.V. Zalamai, Optical spectra of TlGaS2 crystals, J. Lumin. 172 (2016) 111–117, https://doi.org/10.1016/j.jlumin.2015.12.001.

[19] I.G. Stamov, N.N. Syrbu, V.V. Ursaki, V.V. Zalamai, Birefringence and excitonic spectra of TlGaS2 crystals, Opt Commun. 298–299 (2013) 145–149, https://doi.org/10.1016/j.optcom.2013.02.019.

[20] G.E. Delgado, A.J. Mora, F.V. Pérez, J. González, Crystal structure of the ternary semiconductor compound thallium gallium sulfide, TlGaS2, Phys. B Condens. Matter 391 (2007) 385–388, https://doi.org/10.1016/j.physb.2006.10.030.

[21] A.M. Ulubey, F.M. Hashimzade, D.A. Huseinova, M.A. Nizametdinova, G. S. Orudzhev, K.R. Allakhverdiev, N.T. YiLdiZ, Lattice dynamics of layered semiconducting compound TlGaS2, Phys. Status Solidi Basic Res. 248 (2011) 181–186, https://doi.org/10.1002/pssb.201046367.

[22] A.F. Qasrawi, N.M. Gasanly, Optoelectronic and electrical properties of TlGaS 2 single crystal, Phys. Status Solidi Appl. Mater. Sci. 202 (2005) 2501–2507, https://doi.org/10.1002/pssa.200521190.

[23] C.-S. Yoon, B.-H. Kim, D.-J. Cha, A.-M. Maksutoglu, F.A. Mikailzade, M. Yu Seyidov, R.A. Suleymanov, E. Balaban, M. Isik, A. Karatay, A.N. Ech-Chergui, N. M. Gasanly, Study of the structural and optical properties of thallium gallium disulfide (TlGaS2) thin films grown via thermal evaporation, Phys. Scripta (2022), https://doi.org/10.1088/1402-4896/ac74f0.

[24] M. Parto, D. Deger, K. Ulutas, S. Yakut, Structure and dielectric behavior of TlSbS2, Appl. Phys. Mater. Sci. Process 112 (2013) 911–918, https://doi.org/10.1007/S00339-012-7446-9.

[25] D. Deger, K. Ulutaş, Yakut, H. Kara, Dielectric properties and ac conductivity of TlSbTe2 thin films, Mater. Sci. Semicond. Process. 38 (2015) 1–7, https://doi.org/10.1016/j.mssp.2015.03.029.

[26] N. Kalkan, S. Yildirim, K. Ulutas, D. Deger, Electrical Switching in TlSbSe 2 Chalcogenide Semiconductors, (n.d.). doi:10.1007/s11664-007-0318-y.

[27] S.N. Mustafaeva, Influence of the composition of (TlGaS2)1–x(TlInSe2)x solid solutions on their physical properties, Semicond, Phys. Quantum Electron. Optoelectron. 20 (2017) 74–78, https://doi.org/10.15407/spqeo20.01.074.

[28] S. Mustafaeva, M. Asadov, E.K.-I. Materials, U, Dielectric and optical properties of TlGa 1− x Er x S 2 (x= 0, 0.001, 0.005, 0.01) single crystals, Inorg. Mater. 49 (2013) (2013) 1175–1179, https://doi.org/10.1134/S0020168513120121.

[29] F. Kremer, A. Schönhals, Broadband Dielectric Spectroscopy, Springer Berlin Heidelberg, Berlin, Heidelberg, 2003. https://10.1007/978-3-642-56120-7.

[30] K. Ulutas, D. Deger, S. Yakut, Thickness dependence of the dielectric properties of thermally evaporated Sb2Te3 thin films, in: J. Phys. Conf. Ser., Institute of Physics Publishing, 2013, https://doi.org/10.1088/1742-6596/417/1/012040.

[31] S.A. Al-Ghamdi, A.A.A. Darwish, A study on the dielectric non-Debye relaxation and ac and dc conductivity characteristics in nanostructured film of 2,7,12,17-tetra-tert-butyl-5,10,15,20-tetraaza-21H,23H-porphyrin, Eur. Phys. J. Plus. 136 (2021) 812, https://doi.org/10.1140/epjp/s13360-021-01808-y.

[32] M. Alzaid, A. Qasem, E.R. Shaaban, N.M.A. Hadia, Extraction of Thickness, Linear and Nonlinear Optical Parameters of Ge 20+x Se 80-x Thin Films at Normal and Slightly Inclined Light for Optoelectronic Devices, 2020, https://doi.org/10.1016/j.optmat.2020.110539.

[33] S. Ahmadi, N. Khemiri, A. Cantarero, M. Kanzari, XPS Analysis and Structural Characterization of CZTS Thin Films Deposited by One-step Thermal Evaporation, 2022, https://doi.org/10.1016/j.jallcom.2022.166520.

[34] Z.A. Alrowaili, A. Qasem, E.R. Shaaban, M. Ezzeldien, Structure and AC electrical characterization for amorphous Se 50 Te 50 thin-film fabricated by thermal evaporation technique, Phys. B. 612 (2021), 412975, https://doi.org/10.1016/j.physb.2021.412975.

[35] E.M. Assim, E.G. El-Metwally, A study on electrical (dc/ac) conductivity and dielectric characteristics of quaternary Ge 50 in 4 Ga 13 Se 33 chalcogenide thin films, J. Non-Cryst. Solids 566 (2021), 120892, https://doi.org/10.1016/j.jnoncrysol.2021.120892.

[36] G. Zhang, D. Brannum, D. Dong, L. Tang, E. Allahyarov, S. Tang, K. Kodweis, J.-K. Lee, L. Zhu, Interfacial polarization-induced loss mechanisms in polypropylene/BaTiO 3 nanocomposite dielectrics, Chem. Mater. 28 (2016), https://doi.org/10.1021/acs.chemmater.6b01383.

[37] T. Prodromakis, C. Papavassiliou, Engineering the maxwell–wagner polarization effect, Appl. Surf. Sci. 255 (2009) 6989–6994, https://doi.org/10.1016/J.APSUSC.2009.03.030.

[38] Xinyue Chen, Jung-Kai Tseng, Imre Treufeld, Matthew Mackey, D.E. Schuele, Ruipeng Li, Masafumi Fukuto, Eric Baer, Lei Zhu, Enhanced dielectric properties due to space charge-induced interfacial polarization in multilayer polymer films, J. Mater. Chem. C 5 (2017) 10417–10426, https://doi.org/10.1039/C7TC03653A.

[39] N. Pradhani, P.K. Mahapatra, R.N.P. Choudhary, Structural and Impedance Analysis of Bi 0.5 Na 0.5 Ti 0.80 Mn 0.20 O 3 Ceramics, 2019, https://doi.org/10.1016/j.ceramint.2019.10.128.

[40] S. Yakut, K. Ulutas, D. Deger, Effect of thickness on the dielectric properties and glass transition of plasma poly(ethylene oxide) thin films, Mater. Sci. Eng. C. 104 (2019), 109962, https://doi.org/10.1016/J.MSEC.2019.109962.

[41] P. Gupta, P. Mahapatra, R. Choudhary, P. ceramics Bi, Structural and Electrical Characteristics of Rare-Earth Modified Bismuth Layer Structured Compounds, 2021, https://doi.org/10.1016/j.jallcom.2020.158457.

[42] K. Dhahri, Dielectric, ac conductivity and modulus studies of sol–gel BaZrO2.9 compound, Phase Transitions (2020) 1–11, https://doi.org/10.1080/01411594.2020.1789917.

[43] S.G. Chavan, A.N. Tarale, D.J. Salunkhe, Synthesis and characterization of strontium-doped barium titanate thin film by dip and dry technique, OPEN ACCESS J. Adv. Dielectr. 11 (2021), 2150002, https://doi.org/10.1142/S2010135X21500028.

[44] S. Kumar Pal, N. Mehta, S.S. Fouad, H.E. Atyia, Dielectric behavior of amorphous thin films of Se-Te-Sn-Ge system, Solid State Sci. 104 (2020), 106289, https://doi.org/10.1016/j.solidstatesciences.2020.106289.

[45] B. Ma, Y. Wang, Y. Chen, Y. Gao, Dielectric property and interfacial polarization of polymer-derived amorphous silicon carbonitride, Ceram. Int. 43 (2017) 12209–12212, https://doi.org/10.1016/J.CERAMINT.2017.06.081.

[46] H. Sun, H. Zhang, S. Liu, N. Ning, L. Zhang, M. Tian, Y. Wang, Interfacial polarization and dielectric properties of aligned carbon nanotubes/polymer composites: the role of molecular polarity, Compos. Sci. Technol. 154 (2018) 145–153, https://doi.org/10.1016/j.compscitech.2017.11.008.

[47] T.W. Dakin, Conduction and polarization mechanisms and trends in dielectric, IEEE Electr. Insul. Mag. 22 (2006) 11–28, https://doi.org/10.1109/MEI.2006.1705854.

[48] N. Bogris, J. Grammatikakis, A.N. Papathanassiou, Dipole and interfacial polarization phenomena in natural single-crystal calcite studied by the thermally stimulated depolarization currents method, Phys. Rev. B 58 (1998) 10319–10325.

[49] R. Mondal, D. Biswas, S. Paul, A.S. Das, C. Chakrabarti, D. Roy, S. Bhattacharya, S. Kabi, Investigation of microstructural, optical, physical properties and dielectric relaxation process of sulphur incorporated selenium-tellurium ternary glassy systems, Mater. Chem. Phys. 257 (2021), 123793, https://doi.org/10.1016/j.matchemphys.2020.123793.

[50] A.S. Farid, N.A. Hegab, E.A. El-Wahabb, H. Magdy, Influence of Sn, in On Ac Electrical Conductivity and Dielectric Relaxation Behavior of Se-Te Chalcogenide Glass Films, (n.d.). doi:10.1007/s12648-022-02415-y.

[51] D. Değer, K. Ulutas, Conduction and dielectric polarization in Se thin films, Vacuum 72 (2003) 307–312, https://doi.org/10.1016/j.vacuum.2003.08.008.

[52] O. Ajili, B. Louati, K. Guidara, Conductivity and dielectric studies on K2SrP2O7 compound, Appl. Phys. Mater. Sci. Process 119 (2015) 1119–1125, https://doi.org/10.1007/s00339-015-9077-4.

[53] M. Coşkun, Polat, F.M. Coşkun, Z. Durmuş, M. Çağlar, A. Türüt, Frequency and temperature dependent electrical and dielectric properties of LaCrO3 and Ir doped LaCrO3 perovskite compounds, J. Alloys Compd. 740 (2018) 1012–1023, https://doi.org/10.1016/j.jallcom.2018.01.022.

[54] F.F. Al-Harbi, A.A.A. Darwish, T.A. Hamdalla, K.F.A. El-Rahman, Structural analysis, dielectric relaxation, and AC electrical conductivity in TlInSe2 thin films as a function of temperature and frequency, Appl. Phys. A 128 (2022) 1–9, https://doi.org/10.1007/S00339-022-05759-8, 2022 1287.

[55] M. Das Pattanayak, L. Biswal, N. Roy, Dielectric Properties, Relaxation and Study of Conduction Process of Ba 0.5 Sr 0.5 Ti 0.99 Sn 0.01 O 3 Ceramics, 2021, https://doi.org/10.1016/j.matpr.2020.12.1089.

[56] P. Ganga, R. Achary, R. Narayan, P. Choudhary, S. Kumar Parida, Processing and Application of Ceramics 14 (2020) 146–153, https://doi.org/10.2298/PAC2002146A.

[57] S. Yakut, K. Ulutas, D. Deger, Plasma discharge power dependent AC conductivity of plasma poly(ethylene oxide) thin films, Thin Solid Films 645 (2018) 269–277, https://doi.org/10.1016/j.tsf.2017.10.048.

[58] M. Coskun, O. Polat, F.M. Coskun, Z. Durmus, M. Caglar, A. Turut, The influence of cobalt (Co) doping on the electrical and dielectric properties of LaCr1-xCoxO3 perovskite-oxide compounds, Mater. Sci. Semicond. Process. 109 (2020), 104923, https://doi.org/10.1016/j.mssp.2020.104923.

[59] C. Ben Mohamed, K. Karoui, M. Tabellout, A. Ben Rhaiem, Electrical, dielectric and optical properties of [C2H5NH3]2ZnCl4compound, J. Alloys Compd. 688 (2016) 407–415, https://doi.org/10.1016/j.jallcom.2016.07.035.

[60] A. Benali, M. Bejar, E. Dhahri, M.F.P. Graça, L.C. Costa, Electrical conductivity and ac dielectric properties of La0.8Ca0.2-xPbxFeO3 (x = 0.05, 0.10 and 0.15) perovskite compounds, J. Alloys Compd. 653 (2015) 506–512, https://doi.org/10.1016/j.jallcom.2015.09.018.

[61] A. Benali, A. Souissi, M. Bejar, E. Dhahri, M.F.P. Graça, M.A. Valente, Dielectric properties and alternating current conductivity of sol-gel made La0.8Ca0.2FeO3 compound, Chem. Phys. Lett. 637 (2015) 7–12, https://doi.org/10.1016/j.cplett.2015.07.041.

[62] M.A.-E. Salam, H.M. El-Mallah, D.G. El-Damhogi, E. Elesh, Thermal Analysis, Dielectric Response and Electrical Conductivity of Silicon Phthalocyanine Dichloride (SiPcCl 2) Thin Films, (n.d.). doi:10.1007/s11664-020-08604-x.

[63] R. Mguedla, A. Ben, J. Kharrat, M. Saadi, K. Khirouni, N. Chniba-Boudjada, W. Boujelben, Structural, Electrical, Dielectric and Optical Properties of PrCrO 3 Ortho-Chromite, 2019, https://doi.org/10.1016/j.jallcom.2019.152130.

[64] S.I. Qashou, Dielectric Relaxation Properties, and AC Conductivity of Erbium(III)-Tris (8-hydroxyquinolinato) Nanostructured Films, 2022, https://doi.org/10.1016/j.physb.2022.414421.

[65] Y. Shim, T. Kawabata, K. Wakita, N. Mamedov, Temperature behavior of dielectric function spectra and optical transitions in TlGaS2, Phys. Status Solidi Basic Res. 252 (2015) 1254–1257, https://doi.org/10.1002/pssb.201400342.

[66] A. Abkari, I. Chaabane, K. Guidara, Dielectric properties and study of AC electrical conduction mechanisms by non-overlapping small polaron tunneling model in Bis (4-acetylanilinium) tetrachlorocuprate(II) compound, Phys. E Low-Dimensional Syst. Nanostructures. 83 (2016) 119–126, https://doi.org/10.1016/j.physe.2016.04.029.

[67] K. Auromun, R.N.P. Choudhary, Structural, Dielectric and Electrical Characteristics of Lead-free Scandium Modified Barium Iron Niobate: Ba(Fe 0.5-x Sc X Nb 0.5)O 3, 2020, https://doi.org/10.1016/j.physb.2020.412291.

[68] S.-J. Lee, K.-Y. Kang, S.-K. Han, Low-frequency dielectric relaxation of BaTiO3 thin-film capacitors, Appl. Phys. Lett. 75 (1999) 1784, https://doi.org/10.1063/1.124819.

[69] G.M. Tsangaris, G.C. Psarras, N. Kouloumbi, Electric modulus and interfacial polarization in composite polymeric systems, J. Mater. Sci. 33 (338) (1998) 2027–2037, https://doi.org/10.1023/A:1004398514901, 1998.

[70] W.A. Abd El-Ghany, A M Salem, N.H. Teleb, Electrical Properties of Amorphous Ge 26 in X Se 74-x Chalcogenide Thin Films, vol. 128, 2022, p. 504, https://doi.org/10.1007/s00339-022-05615-9.

[71] H. Küçükçelebi, H. Durmuş, A. Deryal, M. Taşer, N. Karakaya, Activation energy of polarization due to electrical conductivity and dipole rotation in purified ca-bentonite, Appl. Clay Sci. 62–63 (2012) 70–79, https://doi.org/10.1016/J.CLAY.2012.04.007.

[72] E.F.M. El-Zaidia, E.A. El-Shazly, H.A.M. Ali, Estimation of electrical conductivity and impedance spectroscopic of bulk CdIn2Se4 chalcogenide, J. Inorg. Organomet. Polym. Mater. 30 (2020) 2979–2986, https://doi.org/10.1007/S10904-020-01454-4/FIGURES/10.

[73] S. Yadav, A.K. Singh, M.K. Roy, Y.S. Katharria, Dielectric and Structural Properties of Pure and Sn-Mixed Ga 2 O 3 Compounds, 2023, https://doi.org/10.1007/s10854-023-10010-y.

[74] V. Galeano, V.H. Zapata, C. Ostos, O. Morán, On the electrical properties of textured YBaCo 2 O 5+δ thin layers tested by means of complex impedance spectroscopy, Vacuum 181 (2020), 109595, https://doi.org/10.1016/j.vacuum.2020.109595.